Int J Legal Med (2011) 125:417–425
DOI 10.1007/s00414-010-0544-3

ORIGINAL ARTICLE

# Age and gender-dependent bone density changes of the human skull disclosed by high-resolution flat-panel computed tomography

**Christina Schulte-Geers · Martin Obert · René L. Schilling · Sebastian Harth · Horst Traupe · Elke R. Gizewski · Marcel A. Verhoff**

Received: 21 October 2010 / Accepted: 20 December 2010 / Published online: 15 January 2011


**Abstract**
*Introduction* The objective of this article was to estimate the age at death in forensic or anthropologic applications based on human skull investigation. Sex-dependent differences were analyzed.
*Methods* Digital, high-resolution, flat-panel-based volumetric computed tomography (eXplore Locus Ultra scanner) images (165,920) of 244 European human skulls–163 males, 81 females–were analyzed according to their radiological bone density, based on Hounsfield units (*H*) that are directly related to the x-ray attenuation of the scanned material. Data were collected by the Department of Forensic Medicine at the University Hospital Giessen and Marburg during 2007 and 2008. Correlation analysis was used for data description.
*Results* Human skull density estimates are widely scattered as a function of age for both sexes. Male skull bone density remains constant during lifetime, whereas female skull bone density decays slowly from approximately 20 years onwards.
*Conclusions* Bone density decay only theoretically provides a new method to determine age at death for adult females. Due to the scattering of the data, an accuracy of approximately ±18 years is found at a confidence interval of 75%, which is, unfortunately, of limited practical interest. We found new sex differences of bone density decay in the skull that are potentially of relevance for the general understanding of bone degradation processes.

**Keywords** Age at death determination · Hounsfield unit density distribution · Bone density · Sex differences · Flat-panel volumetric computed tomography

C. Schulte-Geers · M. Obert · H. Traupe · E. R. Gizewski
Department of Neuroradiology, UKGM, Justus-Liebig University,
Klinikstraße 29,
35385 Giessen, Germany

R. L. Schilling
Institute for Mathematical Stochastics,
TU Dresden, Zellescher Weg 12-14,
01062 Dresden, Germany

S. Harth · M. A. Verhoff
Department of Forensic Medicine, UKGM,
Frankfurter Straße 58,
35392 Giessen, Germany

M. Obert (✉)
Department of Neuroradiology,
University Clinic Giessen and Marburg (UKGM),
Klinikstraße 29,
35385 Giessen, Germany
e-mail: martin.obert@radiol.med.uni-giessen.de

## Introduction

Estimating the age at death (aad) is an important challenge in many civil, forensic, and anthropological problems [1]. The numerous attempts that are devoted to this matter differ, e.g., in the age ranges to which they can be applied. Properties that reflect the development of the growing human organism can be applied in an age range from birth to approximately 20 years [2–7]. Beyond that age range, methods must be applied that are capable of describing processes of degradation of the human body. Bone density decay of the femur can be used for adults; see for instance [8, 9]. Rios et al. [10] used the degree of fusion at the anterior aspect of the sacral vertebrae of adults for aad analysis. Pasquier and colleagues [11] used CT images to investigate pubic bones. They investigated metric anatomical properties defined earlier by Suchey-Brooks [12] and indicated errors for the aad estimation in a range from 7.3 to

11.6 years. Ferrant et al. [13] investigated CT images of coxal bones and performed anatomic measurements. Other methods try to estimate aad in all age ranges. Meinl and coworkers [14] reported an analysis of human tooth cementum annulation and found errors in the estimation of aad in a range of 9.4 to 15.9 years. Others [15, 16] used arterial and dental aspartic acid racemization for aad estimates. Basing the aad estimation on the analysis of bone material has the advantage that bone belongs to the longest-lasting remains of the human body. Among the advantages of computer tomography methods are the nondestructive character of the analysis, the rather quick analysis of the specimen (less than 1 h each), and the generation of digital data, which can be numerically processed by automated image analysis methods. To exploit these advantages, we earlier scanned skull data with a high-resolution flat-panel-based volumetric computed tomography system, the eXplore Locus Ultra (eLU) [17, 18] to investigate whether the degree of closure of the sagittal suture can be used for aad determination; this, however, turned out to be rather ineffective [19, 20].

In this article, we reinvestigated that skull data and developed software that automatically determined the x-ray attenuation-related bone density of the skulls. This density was analyzed according to sex and age in order to find out if there exists a correlation between these parameters that allows giving an estimate of aad.

## Materials and methods

### Human specimens

Two hundred and forty-four human skulls of European ancestry were radiologically investigated in cooperation between the Department of Forensic Medicine and the Department of Neuroradiology of the University Clinic Giessen and Marburg. Skulls were extracted, carefully cleaned, radiologically investigated, and placed back into the human body during autopsy. The procedure was approved by the ethical committee of the University Hospital. See [20] for a detailed description.

### eXplore Locus Ultra, scan parameter, and image reconstruction

The radiological investigation was performed with an eLU, a volumetric microcomputer tomography system, developed by GE Healthcare, London, Ontario, Canada. A detailed description of the system and the applied scan protocol is given in [20]. The CT scanner uses a flat-panel detector (GE Medical Systems, Milwaukee, WI, USA) for radiation detection, which is the basis for the high resolution of the field of view (FOV) of 151.04×151.04×100.30 $mm^3$. One thousand views were taken in one gantry rotation of 16-s duration at 140 kVp and 10 mA. All skulls exceeded a length of 10 cm in the z direction, which is the direction of the table movement, or the anterior-to-posterior direction of a skull that can be imaged by the eLU within one scan. Therefore, the frontal and occipital parts of the skull were scanned separately in two half scans; see Fig. 1. The data were reconstructed with a cone-beam filtered back-projection algorithm into a 512×512×340-voxel matrix, where a voxel is the smallest picture element in a volumetric image data set. The DICOM images that were created have an isotropic voxel size of $(0.295\ mm)^3$. The scanner calibration was monitored frequently during the data acquisition period of the study.

### Numerical evaluation of the parameters volume (*V*), mass (*M*), and density (*D*)

In a CT data set, the Hounsfield unit scale, *H*, describes the gray level of a voxel. The higher the radiological density of a material, the higher is the x-ray attenuation and the higher is the numerical value of *H*. We define the skull volume, *V*, of a structure in a CT data set as the sum of all voxels of the

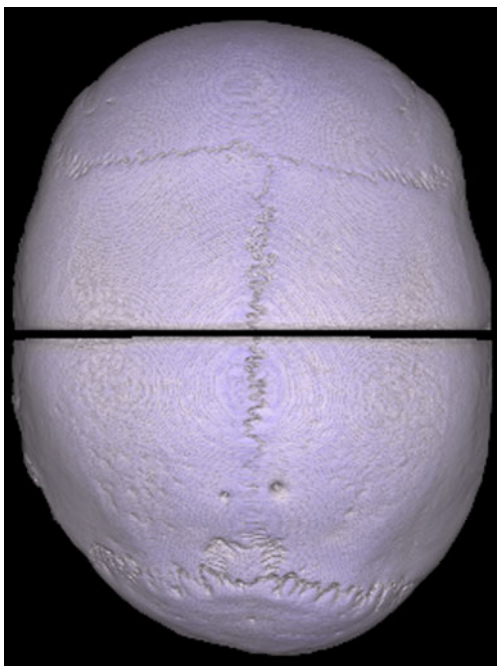

**Fig. 1** Extracranial volume rendering images of a skull of an individual specimen. Due to the limitation of the scanned FOV in the z direction, based on the limited z coverage of the CT system, the direction from bottom to top of the shown image of roughly 10 cm, the frontal (*top of image*) and occipital regions (*bottom of image*) of the skull are taken in two separate scans, which are visible by the horizontal dissection of the skull in the image center. The shown surface rendering is produced with an Advantage Workstation, version 4.1, GE Medical Systems, Buc, France

skull times a scale factor, where the scale factor is known from the isotropic voxel size of the image data reconstruction process. We define the mass, $M$, of a voxel as the Hounsfield unit ($H$) of a voxel, which is linearly related to the attenuation of x-rays within a CT image. We define the density as mass per volume within a scanned image: $D=M/V$. We developed software that enabled the automatic evaluation of the radiological density of a skull. The first step in the estimation of the radiological bone density–abbreviatorily called "density"–of the skull structure in an image data set is to separate the voxels that belong to the skull from those that do not belong to it. The part that represents the structure of the skull is the bone structure itself; parts that do not belong to the skull may be soft tissue that is attached to the skull or parts of the specimen holder of the CT table. The process of identification of the skull structure is called segmentation. The segmentation could be easily performed, taking advantage of the property that all voxels that belong to the skull have x-ray attenuations much larger than, approximately, 300 H. Vice versa, all voxels that do not belong to the skull have a lower $H$ value. Therefore, the identification of the skull could be achieved by a simple threshold method: select all voxels $v$ with $H$ values larger than $H_{\text{threshold}}$ in an image data set. $H_{\text{threshold}}$ was set to a value of 750 in this analysis. The number of voxels, $v$, larger than $H_{\text{threshold}}$ was counted within each image slice of both half scans of the skull of a specimen. This total number of all $v$ of the complete skull data set is directly proportional to the skull volume $V$. Since the voxel size was known as it was defined in the image reconstruction, the volume could be calculated. Adding up all Hounsfield units, $H_v$, of all voxels, $v$, contributing towards $V$, i.e., of all $v$, such that $H_v > H_{threshold}$ gives the mass, $M$, of the skull: $M = \sum_{H_v > H_{threshold}} H_v$. Dividing $M$ by $V$ gives $D$, in units of Hounsfield per cubic millimeters, $D = \frac{M}{V}$. Clearly, $V$, $M$, and hence $D$ depend on $H_{\text{threshold}}$.

The parameters $V$, $M$, and $D$ were analyzed separately of male and female data. The known age of each specimen was tabulated when the parameters of a skull was evaluated, so that the age dependence of the parameters $V$, $M$, and $D$ could be investigated.

The numerical analysis of the image data was performed on a Windows-based PC with a 3 GHz Intel® Core™ 2 Duo CPU and 3 GB of RAM. The software used was written in Interactive Data Language (IDL) version 6.0, RSI, Boulder, CO, USA [21].

## Age-at-death estimation statistic

Regression statistics were calculated to estimate the probability of correlation between the various parameters as functions of age (Pearson and Spearman's rank correlations). The significance test and confidence interval (CI) for the slope of the regression line and the significance of the sample correlation coefficient $r$ were calculated of the functions $V_{(\text{age})}$, $M_{(\text{age})}$, and $D_{(\text{age})}$. See [22] for a detailed description on how to perform the calculations. The Pearson and Spearman's rank correlations were calculated using IDL standard routines [21].

The following set of equations is needed to estimate the prediction accuracy of a newly measured density value of a skull of unknown age at the confidence level $1-\alpha$. See the references [23, 24] for a detailed description of the statistical methodology. The value $x$ corresponds to the density, and $y$, to the age. Equation 1 shows the standard regression line where $b_0$ is the intercept, $b_1$ is the slope, and $\hat{y}$ is the prediction value of age for a measured density $x$.

$$\hat{y} = b_0 + b_1 x \tag{1}$$

Intercept and slope are estimated by Eqs. 2 and 3.

$$b_0 = \bar{y} - b_1 \bar{x} \tag{2}$$

$$b_1 = \frac{s_{yx}}{s_x^2} \tag{3}$$

The empirical averages of $x$ and $y$ are given by Eqs. 4 and 5 for the number of $n$ studied specimens.

$$\bar{x} = \frac{1}{n} \sum\nolimits_{\mathrm{j}=1}^{n} x_{\mathrm{j}} \tag{4}$$

$$\bar{y} = \frac{1}{n} \sum\nolimits_{\mathrm{j}=1}^{n} y_{\mathrm{j}} \tag{5}$$

The empirical covariances are defined by Eqs. 6 through 9,

$$s_{xy} = s_{yx} = \frac{1}{n-1} \sum\nolimits_{\mathrm{j}=1}^{n} \left(x_{\mathrm{j}} - \bar{x}\right)\left(y_{\mathrm{j}} - \bar{y}\right) \tag{6}$$

$$s_x^2 = \frac{1}{n-1} \sum\nolimits_{\mathrm{j}=1}^{n} \left(x_{\mathrm{j}} - \bar{x}\right)^2 \tag{7}$$

$$s_y^2 = \frac{1}{n-1} \sum\nolimits_{\mathrm{j}=1}^{n} \left(y_{\mathrm{j}} - \bar{y}\right)^2 \tag{8}$$

$$s^2 = \frac{1}{n-2} \sum\nolimits_{\mathrm{j}=1}^{n} \left(y_{\mathrm{j}} - \hat{y}_{\mathrm{j}}\right)^2 \tag{9}$$

where $\hat{y}_j$ can be obtained by the regression line, Eq. 10,

$$\hat{y}_{\mathrm{j}} = b_0 + b_1 x_{\mathrm{j}}. \tag{10}$$

The prediction interval is given by term 11,

$$\left[\widehat{y}_0 - t_{\frac{\alpha}{2};n-2}\cdot s\cdot\sqrt{1+\frac{1}{n}+\frac{(x_0-\bar{x})^2}{(n-1)s_x^2}};\widehat{y}_0 + t_{\frac{\alpha}{2};n-1}\cdot s\cdot\sqrt{1+\frac{1}{n}+\frac{(x_0-\bar{x})^2}{(n-1)s_x^2}}\right] \tag{11}$$

$t_{\frac{\alpha}{2};n-2}$ is the Student quantile for a chosen confidence level of $1-\alpha$ of a two-sided test for $n-2$ degrees of freedom.

Investigated specimens

We investigated 163 skulls of males (326 half scans) and 81 female skulls (162 half scans), which give a total of 488 half scans of 244 different specimens. A total number of 165,920 CT images have been analyzed of all specimens.

## Results

Examples of coronal high-resolution CT images are shown in Fig. 2. The different sections through the skull show the diversity of human skulls. The lamina externa has a higher density compared to the lamina interna. The trabecular bone structure is clearly visible. The images show that the segmentation process and the identification of the skull structure were successful. No parts except bone structure can be seen, and no skull parts are missing.

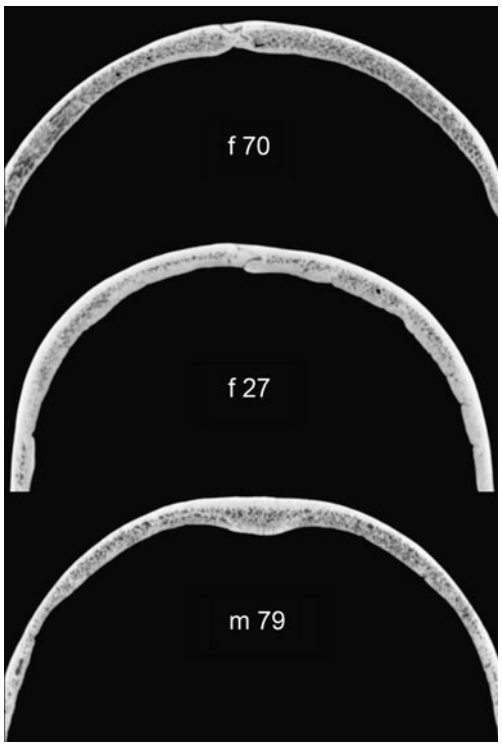


**Fig. 2** Examples of coronal skull images. The label shown below each coronal section indicates sex, *f* female, *m* male, and *age in years*. A width of 13 cm is displayed of each axial skull image. An identical "window width value" of 2,100 *H* and a "window level value" of 700 *H* were used to display the images. The values "window width" and "window level" define the visibility range and center in units of *H* within the Hounsfield unit scale of a CT image. The application of identical values of "window width" and "window level" of all skull images enables a visual comparison of the different images

The frequency distribution of the ages of the specimens of our investigation can be seen in Table 1. The majority of the specimens for the males were in the age range from 30 to 70 years, and for the females, in the range from 50 to 90 years, with significantly less specimens in all other age ranges, which reflects the heterogeneous age distribution of the cases studied by the forensic department of our clinic.

The correlation coefficients of the parameters *V*, *M*, and *D* as function of age for both sexes are summarized in Table 2. They are calculated for an age range from 20 years onwards and older. No correlation between volume, mass, and density as a function of age could be found for males, which was indicated by correlation coefficients that are rather close to zero. For females, we find a weak negative correlation of volume and mass as a function of age, which is expressed in correlation coefficients smaller than −0.5. The female skull density decays slightly as a function of time, which is indicated by a correlation coefficient of −0.6. This decay is already present at an age of roughly 20 years.

The evaluation of age as a function of density is shown for males and females in Fig. 3 in more detail. We estimated the significance of the sample correlation coefficient *r*. The null hypothesis is such that populations x and y have no correlation. For the male population, we find, for a significance at the 1% level, that $r_{\text{critical}}=0.208$. $r_{\text{computed}}=-0.082$. Since $|r_{\text{computed}}|$ does not exceed $r_{\text{critical}}$, we cannot reject $H_0$. Hence, we have no reason to assume a correlation between the two parameters, density and age of the males. For the female specimens, we find, for a significance at the 1% level, that $r_{\text{critical}}=0.302$. $r_{\text{computed}}=-0.623$. Since

**Table 1** Age distribution of investigated specimens

| Age range (years) | Males | Females |
|---|---|---|
| 0 to 9 | 5 | 4 |
| 10 to 19 | 3 | 1 |
| 20 to 29 | 14 | 7 |
| 30 to 39 | 25 | 8 |
| 40 to 49 | 41 | 5 |
| 50 to 59 | 31 | 11 |
| 60 to 69 | 27 | 11 |
| 70 to 79 | 7 | 12 |
| 80 to 89 | 7 | 18 |
| 90 to 99 | 2 | 4 |
| 100 to 109 | 1 | 0 |
| Total | 163 | 81 |

**Table 2** Results of the correlation analysis. Correlation analysis of volume (cubic millimeters), mass (*H*), and density (Hounsfield units per cubic millimeters) of male and female skulls as function of age. Correlations are estimated in the age range of 20 years and older. Correlation coefficients indicate the Pearson correlation coefficient and Spearman's (rho) rank correlation coefficient, respectively

| Parameter of investigation | Pearson correlation coefficient | Spearman's (rho) rank correlation | Two-sided significance of its deviation from zero |
|---|---|---|---|
| $V_{male}$ | −0.15 | −0.16 | 0.045 |
| $M_{male}$ | −0.16 | −0.19 | 0.020 |
| $D_{male}$ | −0.08 | −0.11 | 0.17 |
| $V_{female}$ | −0.33 | −0.35 | 0.0020 |
| $M_{female}$ | −0.46 | −0.49 | $7.0\times10^{-6}$ |
| $D_{female}$ | −0.62 | −0.67 | $5.0\times10^{-11}$ |

$|r_{computed}|$ exceeds $r_{critical}$, we reject $H_0$. Hence, it is reasonable to assume a correlation between the two parameters at the level of 1% significance.

We calculated the significance test and confidence interval for the slope of the regression line. For the male data, we find: degrees of freedom, $f$=155−2=153. $t_{\alpha/2,\ n-2}$= $t_{0.025,\ 153}$=1.976, $|t_{computed}|$=1.022. Since 1.022 does not exceed 1.976, we cannot reject the null hypothesis at a significance level $\alpha$ of 5%. For the female data, we find: degrees of freedom=$f$=76−2=74. $t_{\alpha/2,\ n-2}=t_{0.025,\ 74}$=1.993, $|t_{computed}|$=6.843. Since 6.843 exceeds 1.992, we reject the null hypothesis at the significance level $\alpha$ of 5%.

The scatter plots in Figs. 3 and 4 include prediction intervals at confidence levels of 75%, 90%, and 95%. The decay of the female skull bone density theoretically enables the development of a method of age estimation, where the regression line of the collected data shown in Figs. 3 and 4 can be used as a calibration line. For a given value of *D*, one can read off the corresponding age from the graph in Figs. 3 or 4. The prediction intervals indicate the limits for individual observations of the density on the age in this graph at different confidence intervals. We find an accuracy that corresponds to an error range of approximately ±18, ±26, and ±32 years for confidence intervals of 75%, 90%, and 95%. Table 3 summarizes the results.

All investigations were conducted with an $H_{threshold}$ of 750. Variation of $H_{bone\ threshold}$ in the range from 400 to 900 H has only marginal effects on the correlation results. Clearly, the density rises if the threshold is raised that is used to define the bone volume.

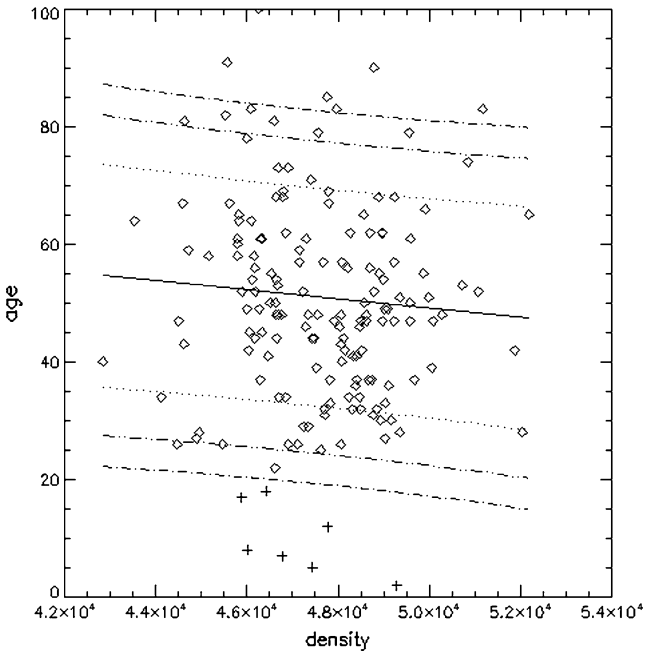


**Fig. 3** Scatter plot of density versus age for men. Shown is the age in years as function of density, *D*, in units of Hounsfield per cubic millimeters, the regression line (*solid line*), and the prediction intervals for individual observations at 75% (*dotted line*), 90% (*slash-dot-dot line*), and 95% confidence limits (*slash-dot line*) for the regression ordinates. The set of 163 males in the age range of 0 to 100 is plotted. The subset of 155 males in the age range of 20 to 100 was used to calculate he statistics. *Crosses* are used for data in the age range of 0 to 19 years, *squares* represent specimens of 20 years or older

## Discussion

The Spearman's statistic was used as it may be applied independently of the distributional properties of the

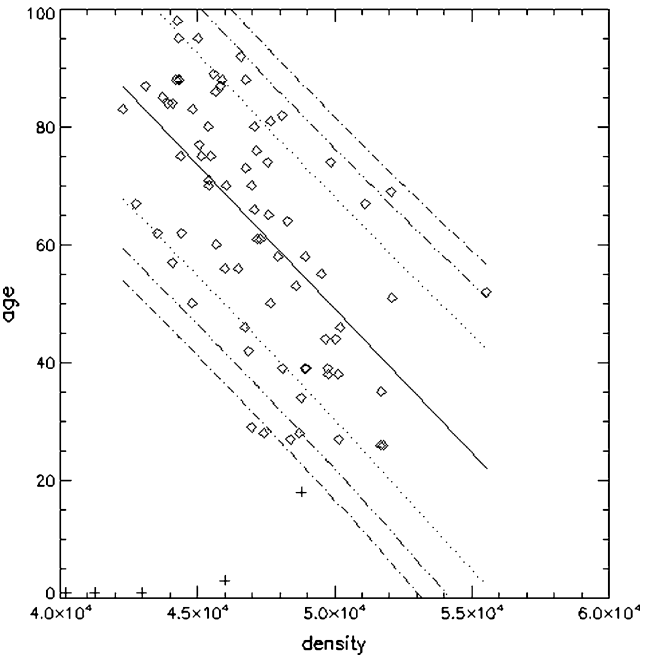


**Fig. 4** Scatter plot of density versus age for women. *Line shapes* and *symbols* are used as described in Fig. 3. The total number of 81 female specimens in the age range of 0 to 99 is plotted. Statistics were calculated for the subset of 76 specimens within the age range of 20 to 99

**Table 3** Statistical parameters and results of the prediction interval estimates of the data shown in Figs. 3 and 4. The approximate error of the age for males or females in units of years is the mean difference between the regression line and the corresponding confidence limit of $p$=75%, 90%, or 95% shown in Figs. 3 and 4

| Statistical parameters | Men | Women |
|---|---|---|
| Number of specimens within age range 20 years and older, $n$ | 155 | 76 |
| Degrees of freedom, $f$, with $f=n-2$ | 153 | 74 |
| Student quantile, $t_{\alpha/2}$ (CI=75%, $\alpha$=0.25, $\alpha/2$=0.125) | 1.15473 | 1.15945 |
| Approximate error (years) for CI=75% | 18.5 | 18.7 |
| Student quantile, $t_{\alpha/2}$ (CI=90%, $\alpha$=0.10, $\alpha/2$=0.050) | 1.65487 | 1.66571 |
| Approximate error (years) for CI=90% | 26.5 | 26.8 |
| Student quantile, $t_{\alpha/2}$ (CI=95%, $\alpha$=0.05, $\alpha/2$=0.025) | 1.97559 | 1.99254 |
| Approximate error (years) for CI=95% | 31.6 | 32.1 |
| Average density, $x_{\text{average}}$ | 47,618.9 | 47,127.0 |
| Average age, $y_{\text{average}}$ | 50.97 | 63.22 |
| $s_{xy}$ | −2,230.0 | −33,066.9 |
| $s^2_x$ | 2,861,746.3 | 6,764,308.3 |
| $s^2_y$ | 256.2 | 417.1 |
| $s$ | 16.00 | 16.09 |
| $s^2$ | 256.1 | 258.9 |
| Intercept, $b_0$ | 88.08 | 293.6 |
| Slope, $b_1$ | −0.0007792 | −0.004888 |

investigated data. We found that there is basically no difference between the Pearson correlation coefficients and Spearman's rank correlation. This shows that there is basically no influence of the inhomogeneous age distribution of our sample as compared to a uniform distribution, which is of statistical relevance. The smaller the two-sided significance of the deviation from zero, the more reliable is the Spearman's rank correlation coefficient. The significance of the deviation of zero is–especially of the female data–so small, that the reliability of the found correlation is unambiguous. The reliability of the male density versus age correlation is smaller if compared to women, although there are nearly twice as many males as females. This sample size effect was discussed already in detail in reference [20]. In the context discussed there, it turned out that, with 95% certainty, a correct $p$ value differs from our estimates by at most 8% for the males and 11% for the females with respect to the sample size. The statement of noncorrelating density for male skulls and a correlation for female skulls as a function of age is supported furthermore by the additional correlation calculations that were carried out.

The data of specimens younger than 20 years were excluded from the correlation analysis. The age range from newly born and young adult specimen contains the period of adolescence and the development of the chondrocranium [25]. Therefore, the exclusion of the data of this age range seems reasonable.

Our hypothetical assumption to estimate aad based on the radiological bone density of human skulls collapsed, in general, as there is no correlation between adult male skull density and age at all. Although there exists a weak correlation among these parameters for adult female skulls, the large error range of approximately ±26 years at a confidence level of 90% of the method denotes why it is of limited practical use.

The reason for the principal difference between male and female skull density behavior is unknown. To the best of our knowledge, this is the first report that shows the sex difference in the skull, based on bone density estimates. So far, mainly metric skull properties are used to discriminate sex; see [26, 27].

It is interesting to note that the linear decay of the bone density is already present with a 20-year-old female specimen in our study. So far, the decay of female bone density found in the literature is reported to start at a much older age of approximately 50 years in other bones [28–30]. Guglielmi et al. analyzed, e.g., the density of the spinal trabecular bones of an Italian population by quantitative computed tomography [31]. They found a rate of bone loss for females of 1.7% per year and of 1.5% for males estimated over an age range from 30 to 85 years. A higher loss of trabecular bone material after an age of 50 years occurs in both sexes, but more severely in females than in males. Estrogen-related changes in the female body, correlated to menopause at that age, are assumed to be responsible to cause that decay. Since the decay of estrogen occurs at approximately 50 years, other effects must be responsible for the decay of bone density that we discovered in the skull at an age of 20 years. Processes that lead to bone density decay seem to be different in different bones. The situation in the skull seems to be different compared to the femur or the spine. If one wants to cure the density loss in the skull, it might turn out that this is possible only during the first 20 years of life when

bone density is built up and rising. Further investigations of this matter might be of interest for the understanding of bone degrading processes like osteoporosis. Future investigations should try to overcome the heterogeneous age distribution of the female skulls of our forensic population; see Table 1. There are 20 female skulls in the age range from 20 to 49 years; 56 skulls are in the age range from 50 years and older. As the data is highly scattered, this might affect our finding of the early decrease of skull density beginning already at a 20-year-old specimen. A larger number of specimens are needed to investigate precisely the age range within which the bone density decrease begins.

We assume that the results of this investigation do not depend on the extremely high resolution and the excellent image quality of the flat-panel CT, visualizing the fine details in bone. A comparison of the high-resolution image quality of the eLU flat-panel CT with a conventional clinical multidetector CT scanner of the skull can be seen in reference [18]. The image quality of state-of-the-art clinical scanners is already sufficient for a reliable bone density analysis. Indeed, there exists a large amount of literature that is related to bone density estimations as function of human age in radiology. For many decades, the decay of bone mass and bone density are, in general, related to fracture risk in the context of osteoporosis and not to aad analysis with a forensic or anthropological background [32]. Most studies concentrated on density measurements of the femur or of vertebrae [31, 33–37]. Special techniques, e. g., dual energy CT, have been developed, devoted to study bone density estimates long ago [38–40]. It is known from those studies that bone density varies as a function of age and sex for different populations and ethnic groups. Guglielmi et al. report, e.g., that the rate of trabecular bone loss for American females and males was higher compared to that of Italian females and males [31]. Factors that have an influence on bone density are ethnic heritage, physical activity, nutrition, artificial hormone uptake, contraceptive drugs, alcohol, and nicotine uptake [41–48]. We assume that the skull bones, studied by us, are independent of physical activity for all populations except Africans, as they are the only population that carries loads on their heads. The other mentioned factors that affect bone density in other bones than the skull may also affect the skull bone density. Their effect contributes possibly to the scattering of our data. It remains to be explored in future studies if it is possible to obtain practically usable aad methods, when more of the contribution of the factors mentioned previously are registered and considered in an evaluation of the skull bone density as a function of age for men and women. Eventually, this enables the optimization of a more complex function that describes the skull bone density as a function of age—reducing the scattering of the data that are related to the bone density.

Johnson [49] describes a multifactorial analysis for age-of-death estimates in 1976, which combined parameters originating from different body properties: tooth status and different cranial suture closure conditions were combined to an estimate of aad, which gave better age predictions. Lovejoy and colleagues [50] expand this attempt and investigated pubic symphyseal face, auricular surface, radiographs of the proximal femur, dental wear, and suture closure in a multifactorial way. We assume that our attempt to investigate skull density can certainly be used as one possible parameter, among others, in such a multifactorial analysis for adult females. Based on the rather recent knowledge that the closure of skull sutures does not correlate with age [16, 20, 51, 52], it seems to be advisable to remove this parameter in any multifactorial aad analysis of adult specimens.

## Conclusion

Based on an analysis of high-resolution CT images, we found that the adult male skull bone density is uncorrelated to age studied in the age range beginning from 20 years onwards. For the female skull, we found a density decay of bone density already present at the age of 20 years. The huge scattering of the density values as function of age prevents the practical application of aad estimates based on that functional dependence for female skulls. The accuracy of an age estimate is just in the range of ±26 years at a confidence level of 90%, which indicates the practical uselessness of the method. These results could potentially lead to better results in a multifactorial aad analysis, where our method provides one parameter–at least for females–among others.

**Acknowledgments** We would like to thank Nicole Graf and Manfred Benner for the preparation of the skull specimen. We thank Sehib Tuerkay, Barbara Ahlemeyer, and Manfred Sernetz for helpful discussions.

## References

1. Cunha E, Baccino E, Martrille L, Ramsthaler F, Prieto J, Schuliar Y, Lynnerup N, Cattaneo C (2009) The problem of aging human remains and living individuals: a review. Forensic Sci Int 193:1–13
2. Kellinghaus M, Schulz R, Vieth V, Schmidt S, Pfeiffer H, Schmeling A (2010) Enhanced possibilities to make statements on the ossification status of the medial clavicular epiphysis using an amplified staging scheme in evaluating thin-slice CT scans. Int J Leg Med 124:321–325
3. Schmidt S, Nitz I, Schulz R, Schmeling A (2008) Applicability of the skeletal age determination method of Tanner and Whitehouse for forensic age diagnostics. Int J Leg Med 122:309–314
4. Kellinghaus M, Schulz R, Vieth V, Schmidt S, Schmeling A (2010) Forensic age estimation in living subjects based on the

ossification status of the medial clavicular epiphysis as revealed by thin-slice multidetector computed tomography. Int J Leg Med 124:149–154
5. Knell B, Ruhstaller P, Prieels F, Schmeling A (2009) Dental age diagnostics by means of radiographical evaluation of the growth stages of lower wisdom teeth. Int J Leg Med 123:465–469
6. Olze A, Solheim T, Schulz R, Kupfer M, Pfeiffer H, Schmeling A (2010) Assessment of the radiographic visibility of the periodontal ligament in the lower third molars for the purpose of forensic age estimation in living individuals. Int J Leg Med 124:445–448
7. Olze A, Solheim T, Schulz R, Kupfer M, Schmeling A (2010) Evaluation of the radiographic visibility of the root pulp in the lower third molars for the purpose of forensic age estimation in living individuals. Int J Leg Med 124:183–186
8. Macchiarelli R, Bonduoli L (1994) Linear densitometry and digital image processing of proximal femur radiographs: implications for archaeological and forensic anthropology. Am J Phys Anthropol 93:109–122
9. Rissech C, Schaefer M, Malgosa A (2008) Development of the femur–implications for age and sex determination. Forensic Sci Int 180:1–9
10. Ríos L, Weisensee K, Rissech C (2008) Sacral fusion as an aid in age estimation. Forensic Sci Int 180:111.e1–111.e7
11. Pasquier E, De Saint Martin Pernot L, Burdin V, Mounayer C, Le Rest C, Colin D, Mottier D, Roux C, Baccino E (1999) Determination of age at death: assessment of an algorithm of age prediction using numerical three-dimensional CT data from pubic bones. Am J Phys Anthropol 108:261–268
12. Brooks S, Suchey JM (1990) Skeletal age determination based on the os pubis: a comparison of the Acsàdi-Nemeskéri and Suchey-Brooks methods. Hum Evol 5:227–238
13. Ferrant O, Rougé-Maillart C, Guittet L, Papin F, Clin B, Fau G, Telmon N (2009) Age at death estimation of adult males using coxal bone and CT scan: a preliminary study. Forensic Sci Int 186:14–21
14. Meinl A, Huber CD, Tangl S, Gruber GM, Teschler-Nicola M, Watzek G (2008) Comparison of the validity of three dental methods for the estimation of age at death. Forensic Sci Int 178:96–105
15. Dobberstein RC, Tung S-M, Ritz-Timme S (2010) Aspartic acid racemisation in purified elastin from arteries as basis for age estimation. Int J Leg Med 124:269–275
16. Dorandeu A, Coulibaly B, Piercecchi-Marti MD, Bartoli C, Gaudart J, Baccino E, Leonetti G (2008) Age-at-death estimation based on the study of frontosphenoidal sutures. Forensic Sci Int 177:47–51
17. Obert M, Ahlemeyer B, Baumgart-Vogt E, Traupe H (2005) Flat-panel volumetric computed tomography a new method for visualizing fine bone detail in living mice. J Comput Assist Tomogr 29:560–565
18. Verhoff MA, Karger B, Ramsthaler F, Obert M (2008) Investigations on an isolated skull with gunshot wounds using flat-panel CT. Int J Leg Med 122:441–445
19. Reuß C, Obert M, Schilling R, Harth S, Traupe H, Verhoff MA (2008) Automatische Analyse von hochauflösenden flat-panel Computertomographie-Bildern zur Bestimmung des Verknöcherungszustandes von Suturen zur Altersbestimmung beim Menschen. 87th Annual conference of the German forensic society, Dresden
20. Obert M, Schulte-Geers C, Schilling RL, Harth S, Kläver M, Traupe H, Verhoff MA (2010) High-resolution flat-panel volumetric CT images show no correlation between human age and suture obliteration–independent of sex. Forensic Sci Int 180:180.e1–180.e12
21. IDL reference guide, version 6.0 (2003) Research Systems Inc., RSI, Boulder, CO, USA
22. Crow EL, Davis FA, Maxfield MW (1960) Statistics manual. Dover Publications, New York
23. Zwillinger D, Kokoska S (2000) CRC standard probability and statistics tables and formulae. Chapman & Hall/CRC, Boca Raton
24. Beichelt FE, Montgomery DC (2003) Teubner-Taschenbuch der Stochastik. Wahrscheinlichkeitstheorie, Stochastische Prozesse, Mathematische Statistik. B.G. Teubner, Stuttgart
25. Madeline LA, Elster AD (1995) Suture closure in the human chondrocranium: CT assessment. Radiology 196:747–756
26. Robinson MS, Bidmos MA (2009) The skull and humerus in the determination of sex: reliability of discriminant function equations. Forensic Sci Int 186:86.e1–86.e5
27. Steyn M, Iscan MY (1998) Sexual dimorphism in the crania and mandibles of South African whites. Forensic Sci Int 98:9–16
28. Steiger P, Cummings SR, Black DM, Spencer NE, Genant HK (1992) Age-related decrements in bone mineral density in women over 65. J Bone Miner Res 7:625–632
29. Ribot C, Tremlliers F, Poullies JM, Louvet JP, Guiraud R (1988) Influence of the menopause and aging on spinal density in French women. Bone Miner 5:89–97
30. Ortolani S, Trevisan C, Bianchi ML, Caraceni MP, Ulivieri FM, Gandolini G, Montessano A, Polli EE (1991) Spinal and forearm bone mass in relation to ageing and menopause in healthy Italian women. Eur J Clin Investig 21:33–39
31. Guglielmi G, Giannatempo GM, Blunt BA, Grampp S, Glüer CC, Cammisa M, Genant HK (1995) Spinal bone mineral density by quantitative CT in a normal Italian population. Eur Radiol 5:269–275
32. Jahng JS, Kang KS, Park HW, Han MH (1991) Assessment of bone mineral density in postmenopausal and senile osteoporosis using quantitative CT. Orthopedics 14:1101–1105
33. Cann CE, Genant HK (1980) Precise measurement of vertebral mineral content using computed tomography. J Comput Assist Tomogr 4:493–500
34. Jones CD, Laval-Jeantet AM, Laval-Jeantet MH, Genant HK (1987) Importance of measurement of spongious vertebral bone mineral density in the assessment of osteoporosis. Bone 8:201–206
35. Nilsson M, Johnell O, Johnsson K, Redlund-Johnell I (1988) Quantitative computed tomography in measurement of vertebral trabecular bone mass. Acta Radiol 29:719–725
36. Kelly PJ, Nguyen T, Hopper J, Pocock N, Sambrook P, Eisman J (1993) Changes in axial bone density with age: a twin study. J Bone Miner Res 8:11–17
37. Cummings SR, Black DM, Nevitt MC, Browner W, Cauley J, Ensrud K, Genant HK, Palermo L, Scott J, Vogt TM (1993) Bone density at various sites for prediction of hip fractures. Lancet 341:72–75
38. Burgess AE, Colborne B, Zoffmann E (1987) Vertebral trabecular bone: comparison of single and dual-energy CT measurements with chemical analysis. J Comput Assist Tomogr 11:506–515
39. Cann CE (1987) QCT applications: comparison of current scanners. Radiology 162:257–261
40. Cann CE (1988) Quantitative CT for determination of bone mineral density: a review. Radiology 166:509–522
41. Tobias JH, Cook D, Chambers TJ, Dalzell N (1993) Low spinal bone mass in Asian women reflects their small skeletal size. J Bone Miner Res 8:S330
42. De Simone DP, Stevens J, Edwards J, Shary J, Gordon L, Bell NH (1989) Influence of body habitus and race on bone mineral density of the midradius, hip and spine in aging women. J Bone Miner Res 4:827–830
43. Luckey MM, Meier DE, Mandeli JP, Da Costa MC, Hubbard MC, Goldsmith SJ (1989) Radial and vertebral bone density in white and black women: evidence for racial differences in premenopausal bone homeostasis. J Clin Endocrinol Metab 69:762–770
44. Harbison J, Daly L, Murphy B, Mc Coy C, Masterson J (1992) Normal bone density in Irish women: is American normative data suitable for use in Ireland? Ir J Med Sci 16:66–69

45. Krall EA, Dawson-Hughes B (1993) Heritable and life-style determinants of bone mineral density. J Bone Miner Res 8:1–9
46. Reid IR, Mackie M, Ibbertson HK (1986) Bone mineral content in Polynesian and white New Zealand women. Brit Med J 292:1547–1548
47. Liel Y, Edwards J, Shary J (1988) Effect of race and body habitus on bone mineral density of the radius, hip, and spine in premenopausal women. J Clin Endocrinol Metab 66:1247–1250
48. Mazess RB, Barden HS (1991) Bone density in premenopausal women: effect of age, dietary intake, physical activity, smoking, and birth-control pills. Am J Clin Nutr 53:132–142
49. Johnson JS (1976) A comparison of age estimation using discriminant function analysis with some other estimations of unknown skulls. J Anat 121:475–484
50. Lovejoy CO, Meindl RS, Mensforth RP, Barton TJ (1985) Multifactorial determination of skeletal age at death: a method and blind tests of its accuracy. Am J Phys Anthropol 68:1–14
51. Hershkovitz I, Latimer B, Dutour O, Jellema LM, Wish-Baratz S, Rothschild C, Rothschild BM (1997) Why do we fail in aging the skull from the sagittal suture? Am J Phys Anthropol 103:393–399
52. Sahni D, Jit I, Neelam S (2005) Time of closure of cranial sutures in northwest Indian adults. Forensic Sci Int 148:199–205